AIAA JOURNAL
Vol. 34, No. 6, June 1996

Coupled Layerwise Analysis of Thermopiezoelectric Composite Beams

Ho-Jun Lee* and Dimitris A. Saravanos†
NASA Lewis Research Center, Cleveland, Ohio 44135

Previously developed discrete layer mechanics are extended to incorporate thermal effects to account for the complete coupled mechanical, electrical, and thermal response of piezoelectric composite beams. Thermal effects in both the elastic and piezoelectric media are captured at the material level. This unified representation leads to an inherent capability to model both the sensory and active responses of piezoelectric composite beams in thermal environments. Finite element equations are developed and implemented for a beam element with linear shape functions. Results from the current formulation are compared with results from a conventional thermoelastic finite element analysis and classical beam theory. Additional numerical studies demonstrate capabilities of the current formulation to predict the thermal deformation of composite beams, as well as the active compensation of these thermal deformations using piezoelectric structures. The corresponding sensory response and the resultant stress state in the piezoelectric composite beam are also presented.

Nomenclature

$[A^{mn}]$, $[B^{mn}]$, $[D^{mn}]$	= generalized laminate matrices
b	= width of beam
$[C]$	= elastic stiffness matrix
$\{D\}$	= electric displacement vector
$[d]$	= piezoelectric tensor
$\{E\}$	= electric field
$[E^{mn}]$	= generalized laminate piezoelectric matrices
$[e]$	= piezoelectric tensor
$\{F\}$	= thermal force vector
$\{f\}$	= generalized laminate thermal force vector
$\{\bar{f}\}$	= body force per unit volume
$[G^{mn}]$	= generalized laminate electric permittivity matrices
$[K]$	= stiffness matrix
$[M]$	= mass matrix
$[P^{mn}]$	= generalized laminate mass matrices
p	= pyroelectric constant
$\{Q\}$	= thermal electric charge
$\{q\}$	= generalized laminate thermal electric displacements
$\bar{q}$	= surface electric charge
R	= in-plane interpolation functions
$\{S\}$	= engineering strain
$[s]$	= elastic compliance
T	= temperature
t	= time
$\{\bar{t}\}$	= surface tractions
u, v, w	= displacements along x, y, z axes, respectively
x, y, z	= structural axes
x_1, x_2, x_3	= material axes
α	= strain coefficient of thermal expansion
δ	= variational operator
$[\epsilon]$	= electric permittivity tensor
θ	= temperature difference from reference temperature
λ	= stress coefficient of thermal expansion
ρ	= density
$\{\sigma\}$	= mechanical stress
ϕ	= electric potential
ψ	= through-the-thickness interpolation function

Subscripts

th	= thermal
uu, $u\phi$, $\phi\phi$	= structural, piezoelectric, and dielectric, respectively
0	= reference conditions
l	= layer or ply

Superscripts

a	= active
E	= constant electric field conditions
S	= constant strain conditions
s	= sensory
T	= constant temperature conditions
σ	= constant stress conditions

Received Feb. 15, 1995; revision received Jan. 30, 1996; accepted for publication Feb. 10, 1996.

*Aerospace Engineer, Structural Mechanics Branch, 21000 Brookpark Road, Mail Stop 23-3. Member AIAA.

†Senior Research Associate, Ohio Aerospace Institute, 22800 Cedar Point Road, Brookpark, OH 44142. Member AIAA.

Introduction

THE development of intelligent composite materials with piezoelectric components offers great potential for use in advanced aerospace structural applications. By taking advantage of the direct and converse piezoelectric effect of embedded piezoceramic or piezopolymer devices, these novel materials can combine the superior mechanical and thermal properties found in conventional composites along with the inherent self-monitoring and adaptive capabilities of piezoelectric materials. An area where such materials may provide dramatic advantages is in the development of piezoelectric composite structures with the capability to sense thermally induced distortions and to actively compensate for adverse thermomechanical conditions. Typical applications of such structures are envisioned in the thermal distortion management of propulsion components and/or space structures. Before they can be utilized in these applications, however, the performance of piezoelectric structures in thermal environments must be quantified. Consequently, this paper will present the development of comprehensive mechanics for the analysis of such piezoelectric thermal composite structures.

Extensive development of analytical methods for modeling the behavior of piezoelectric structures has been reported in the literature. The early works focused mainly on the development of simpli-

fied models for the vibration control of beams.[1,2] This was followed by the extension of classical lamination theory to incorporate piezoelectric effects.[3–5] The development of this piezoelectric laminate theory led, in turn, to the formation of finite element methods for the analysis of smart structures using plate and shell elements.[6–10] In general, classical laminate theory provides acceptable in-plane results for low thicknesses. However, the classical theory neglects interlaminar shear stresses and proves to be inaccurate for analyzing both thick laminates and laminates with strong inhomogeneities. There are two basic approaches taken to develop a refined laminate theory that accounts for the limitations of the classical theory[11]: 1) higher-order theories and 2) discrete layer theories. The higher-order theories provide a relatively simple and computationally efficient alternative to the classical theory, which is sufficient for many applications. However, the common drawback of the higher-order theories is the assumption of continuous transverse strains across the interfaces of different materials, which again leads to inaccurate results for thick laminates and laminates with strong inhomogeneities. These limitations are addressed by the discrete layer theories in which separate displacement fields can be assumed in each layer and provide a generalization of the classical and higher-order theories. However, the increased accuracy of transverse stress predictions comes at the price of increased problem complexity and higher computational costs. The first attempt to implement a discrete layer theory for active beams (based on an induced strain approach) into a finite element formulation was performed by Robbins and Reddy.[12] This discrete layer theory was, in turn, extended to incorporate the coupled equations of piezoelectricity and developed into a multifield finite element formulation for beams and plates by Heyliger et al.[13] and Saravanos and Heyliger.[14]

All of the previously described methods neglect the implications of thermal effects on both the active and sensory response of smart structures. Thermal effects become important when the piezoelectric structure has to operate in either extremely hot or cold temperature environments. These extreme conditions may severely affect the response of piezoelectric structures in three distinct ways: 1) induction of thermal stresses resulting from differences in the coefficients of thermal expansion between the various composite plies and piezoelectric layers, 2) pyroelectric phenomena (i.e., changes in the electrical displacements arising from the coupled electrical and thermal behavior of the piezoelectric material), and 3) temperature dependence of the elastic, piezoelectric, and dielectric properties. Only a limited amount of work has been reported concerning this topic. Mindlin[15] formulated a set of two-dimensional thermopiezoelectric equations for plates. Tauchert[16] extended the classical lamination theory to account for the coupled effects of thermopiezoelectricity. Rao and Sunar,[17] Tzou and Howard,[18] and Tzou and Ye[19] developed finite element formulations for plates and shells (based on classical lamination theory) to account for thermopiezoelectricity.

Consequently, the purpose of this paper is to extend the previously developed discrete layer formulation of Saravanos and Heyliger[14] to account for the coupled mechanical, electrical, and thermal response in modern piezoelectric composite beams. The mechanics account for thermal effects, which may arise in the elastic and piezoelectric media at the material level through the constitutive equations. The displacements, electric potentials, and temperatures are introduced as state variables, allowing them to be modeled as variable fields through the laminate thickness. This unified representation leads to an inherent capability to model both the active compensation of thermal distortions in piezoelectric composite structures and the resultant sensory voltage when thermal loads are applied. The corresponding finite element formulation is developed, and numerical results demonstrate the ability to model both the active and sensory modes of composite beams with heterogeneous plies with an attached piezoelectric layer under thermal loadings.

Governing Material Equations

This section outlines the foundations and steps required for developing the governing equations of composite beams with embedded piezoelectric layers. The mechanical response of the piezoelectric material can be represented by the equation of motion

$$\rho \ddot{u}_i = \sigma_{ij,j} + \bar{f}_i \tag{1}$$

The electrical response of the piezoelectric material is described by the electrostatic (or Maxwell's) equation

$$D_{i,i} = 0 \tag{2}$$

The small deformation strain-displacement relations are

$$S_{ij} = \tfrac{1}{2}(u_{i,j} + u_{j,i}) \tag{3}$$

and the electric field vector is related to the electric potential by

$$E_i = -\phi_{,i} \tag{4}$$

The constitutive equations for a thermopiezoelectric material[20] employing standard contracted notation are

$$S_\alpha = s^{E,T}_{\alpha,\beta}(T)\sigma_\beta + d^T_{\alpha m}(T)E_m + \alpha^{E,T}_\alpha(T)\theta \tag{5}$$

$$D_m = d^T_{m\alpha}(T)\sigma_\alpha + \epsilon^{\sigma,T}_{mk}(T)E_k + p^{\sigma,T}_m(T)\theta \tag{6}$$

or in semi-inverted form

$$\sigma_\alpha = C^{E,T}_{\alpha\beta}(T)S_\beta - e^T_{\alpha m}(T)E_m - \lambda^{E,T}_\alpha(T)\theta \tag{7}$$

$$D_m = e^T_{m\alpha}(T)S_\alpha + \epsilon^{S,T}_{mk}(T)E_k + p^{S,T}_m(T)\theta \tag{8}$$

with

$$\begin{aligned} e^T_{\alpha m}(T) &= C^{E,T}_{\alpha\beta}(T)d^T_{\beta m}(T) \\ \lambda^{E,T}_\alpha(T) &= C^{E,T}_{\alpha\beta}(T)\alpha^{E,T}_\beta(T) \\ \theta &= T - T_0 \\ \epsilon^{S,T}_{mk}(T) &= \epsilon^{\sigma,T}_{mk}(T) - d^T_{m\alpha}(T)e^T_{\alpha k}(T) \\ p^{S,T}_m(T) &= p^{\sigma,T}_m(T) - d^T_{m\alpha}(T)\lambda^{E,T}_\alpha(T) \end{aligned} \tag{9}$$

Through use of the divergence theorem and neglecting body forces, Eqs. (1) and (2) can be expressed in an equivalent variational form as

$$\int_V \rho \ddot{u}_i \delta u_i \, dV + \int_V \sigma_{ij}\delta S_{ij} \, dV - \int_{V_p} D_i \delta E_i \, dV = \int_A \bar{t}_i \delta u_i \, dA + \int_{A_p} \bar{q}\delta\phi \, dA \tag{10}$$

where A and V represent the surface area and the volume of both the composite and piezoelectric materials, respectively, whereas A_p and V_p are the surface area and the volume of only the piezoelectric material.

Discrete Layer Formulation

A discrete layer laminate theory for thermal piezoelectric composite beams is described in this section. For beams, a simplified displacement and electric potential can be obtained since only axial variations of the state variables are assumed:

$$u = u(x,z), \qquad v = 0, \qquad w = w(x,z), \qquad \phi = \phi(x,z) \tag{11}$$

The discrete layer theory implements the following piecewise continuous approximations through the laminate thickness for the state variables:

$$u(x,z,t) = \sum_{j=1}^{n} U^j(x,t)\psi^j(z) \tag{12}$$

$$w(x,z,t) = w^0(x,t) \tag{13}$$

$$\phi(x,z,t) = \sum_{j=1}^{n} \phi^j(x,t)\psi^j(z) \tag{14}$$

$$\theta(z,t) = \sum_{j=1}^{n} \theta^j(t)\psi^j(z) \tag{15}$$

where n is the number of interpolation functions ψ^j and a constant through-the-thickness displacement, w, is assumed. Currently, ψ^j is represented using linear Lagrangian interpolation functions.

By combining Eqs. (3), (7), (8), (10), and (12–15) and integrating through-the-thickness, the following variational form can be obtained:

$$\sum_{k=1}^{n}\sum_{m=1}^{n}\int_x P_{11}^{km}\ddot{u}^m\delta u^k\,dx + \int_x P_{33}\ddot{w}^0\delta w^0\,dx + \sum_{k=1}^{n}\sum_{m=1}^{n}\int_x \left(D_{11}^{km}\frac{\partial u^m}{\partial x}\frac{\partial \delta u^k}{\partial x} + D_{55}^{km}u^m\delta u^k\right)dx + \sum_{k=1}^{n}\int_x B_{55}^{k}\left(\frac{\partial w^0}{\partial x}\delta u^k + u^k\frac{\partial \delta w^0}{\partial x}\right)dx + \int_x A_{55}\frac{\partial w^0}{\partial x}\frac{\partial \delta w^0}{\partial x}dx + \sum_{k=1}^{n}\sum_{m=1}^{n}\int_x E_{31}^{km}\left(\phi^m\frac{\partial \delta u^k}{\partial x} + \frac{\partial u^k}{\partial x}\delta\phi^k\right)dx - \sum_{k=1}^{n}\sum_{m=1}^{n}\int_x G_{33}^{km}\phi^m\delta\phi^k dx - \sum_{k=1}^{n}\int_x \left(f_{l,\mathrm{th}}^{k}\frac{\partial \delta u^k}{\partial x} - q_{\mathrm{th}}^{k}\delta\phi^k\right)dx = \sum_{k=1}^{n}\left[f_1^k\delta u^k + q^k\delta\phi^k\right]_x + \left[f_3\delta w^0\right]_x \tag{16}$$

The discrete layer laminate matrices for the density, stiffness, piezoelectric, electric permittivitty, and external forces of a composite beam have been presented previously in a general form.[13,14] The newly derived resultant laminate thermal force vector is

$$f_{l,\mathrm{th}}^{k} = \sum_{l=1}^{L}\int_x b\lambda_1\theta^j\psi^j(z)\psi^k(z)\,dz \tag{17}$$

and the resultant thermal electric displacement is

$$q_{\mathrm{th}}^{k} = \sum_{l=1}^{L}\int_x bp_3\theta^j\psi^j(z)\frac{\partial\psi^k(z)}{\partial z}\,dz \tag{18}$$

where L is the number of plies.

Finite Element Formulation

The finite element formulation for a composite piezoelectric beam is obtained by incorporating additional local in-plane approximations to the state variables

$$u(x,z,t) = \sum_{i=1}^{m}\sum_{j=1}^{n}U^{ji}(t)R^i(x)\psi^j(z) \tag{19}$$

$$w(x,z,t) = \sum_{i=1}^{m}W^{0i}(t)R^i(x) \tag{20}$$

$$\phi(x,z,t) = \sum_{i=1}^{m}\sum_{j=1}^{n}\phi^{ji}(t)R^i(x)\psi^j(z) \tag{21}$$

where m is the number of in-plane shape functions R. Currently, R is represented using linear Lagrangian interpolation functions and a selectively reduced integration scheme is implemented for the second stiffness term (containing D_{55}) of Eq. (16) to eliminate overstiffening at low thicknesses.

By combining Eqs. (3), (7), (8), (10), (19–21), the following finite element matrix formulation is obtained:

$$\begin{bmatrix}[M_{11}] & 0 & 0\\ 0 & [M_{33}] & 0\\ 0 & 0 & 0\end{bmatrix}\begin{Bmatrix}\ddot{U}\\ \ddot{W}\\ \ddot{\Phi}\end{Bmatrix} + \begin{bmatrix}[K_{11}] & [K_{13}] & [K_{14}]\\ [K_{31}] & [K_{33}] & 0\\ [K_{41}] & 0 & [K_{44}]\end{bmatrix}\times\begin{Bmatrix}U\\ W\\ \Phi\end{Bmatrix} = \begin{Bmatrix}F_1\\ F_3\\ Q\end{Bmatrix} + \begin{Bmatrix}F_{l,\mathrm{th}}\\ 0\\ Q_{\mathrm{th}}\end{Bmatrix} \tag{22}$$

where the elements of the submatrices of Eq. (22) are calculated from the generalized discrete layer laminate matrices. The finite element matrices for the mass, stiffness, and external force have been presented previously in a general form.[13,14] The newly derived finite element thermal force vector is

$$F_{l,\mathrm{th}}^{i} = \int_x f_{l,\mathrm{th}}\frac{\partial R^i(x)}{\partial x}\,dx \tag{23}$$

and the thermal electric charge is

$$Q_{\mathrm{th}}^{i} = -\int_x q_{\mathrm{th}}R^i(x)\,dx \tag{24}$$

By expressing the finite element matrix formulation in a compact form and by partitioning the electric potential vector into active and sensory components such that $\{\phi\} = \{\phi^a; \phi^s\}$, the following partitioned form of Eq. (22) can be obtained:

$$\begin{bmatrix}[M_{uu}] & 0\\ 0 & 0\end{bmatrix}\begin{Bmatrix}\ddot{U}\\ \ddot{\Phi}^s\end{Bmatrix} + \begin{bmatrix}[K_{uu}] & [K_{u\phi}^{ss}]\\ [K_{\phi u}^{ss}] & [K_{\phi\phi}^{ss}]\end{bmatrix}\begin{Bmatrix}U\\ \Phi^s\end{Bmatrix} = \begin{Bmatrix}F + F_{\mathrm{th}} - [K_{u\phi}^{sa}]\Phi^a\\ Q^s + Q_{\mathrm{th}} - [K_{\phi\phi}^{sa}]\Phi^a\end{Bmatrix} \tag{25}$$

This form has the advantage of positioning the unknown variables (displacements and sensory electric potentials) in the left-hand terms, while the known quantities (mechanical loads, thermal loads, electric charges, and active voltages) are included in the right-hand terms.

Equation (25) can then be uncoupled into the following independent equations for the structural displacements:

$$[M_{uu}]\ddot{U} + \left([K_{uu}] - [K_{u\phi}^{ss}][K_{\phi\phi}^{ss}]^{-1}[K_{\phi u}^{ss}]\right)U = F + F_{\mathrm{th}} + \left([K_{u\phi}^{ss}][K_{\phi\phi}^{ss}]^{-1}[K_{\phi\phi}^{sa}] - [K_{u\phi}^{sa}]\right)\Phi^a \tag{26}$$

and the electric potentials at the sensors

$$\Phi^s = -[K_{\phi\phi}^{ss}]^{-1}\left([K_{\phi u}^{ss}]U + [K_{\phi\phi}^{sa}]\Phi^a - Q^s - Q_{\mathrm{th}}\right) \tag{27}$$

Applications

Materials and Assumptions

Results from representative problems are presented in this section to evaluate the discrete layer formulation and to demonstrate the performance of simple sensory/active structures in thermal environments. Two different composite cantilever beam configurations are considered, as shown in Fig. 1. For both cases, the beam is 25.4 cm (10 in.) long and 2.54 cm (1.0 in.) wide and consists of various orientations of graphite/epoxy plies attached to piezoelectric layers, where each graphite/epoxy ply and piezoelectric layer has a thickness of 0.0127 cm (0.005 in.). A total of 30 equally spaced linear beam elements are modeled along the length of the beam, while one discrete layer is used through-the-thickness for each piezoelectric and graphite/epoxy layer. The material properties used for the graphite/epoxy and piezoelectric layers are listed in Table 1. The piezoelectric material used for this study is the commercially available piezoceramic APC 840 (American Piezo Ceramics, Inc., Mackeyville, PA), while representative material properties of a graphite/epoxy composite were selected. The current study neglects the temperature dependence of material properties. The program is written in Fortran 77 and operates on a four processor SUN SPARC-server 1000 UNIX workstation. The accuracy of the beam element developed in this study is verified for both beam configurations examined. The results are shown in Table 2 and indicate the relative insensitivity of this element to the varying aspect ratios for the configurations examined.

$[0_8/p]$ Beam Under Uniform Thermal Load

Thermal Displacements

The first beam considered is a $[0_8/p]$ configuration, where p is the piezoelectric layer, under a uniform thermal load of 100°C. The presence of the piezoelectric layer results in an asymmetric laminate

Table 1 Material properties of piezoelectric composite beam

Property	Graphite/epoxy	Piezoceramic APC 840
Density ρ, g/cm^3 (lb/in.^{3})	2.1 (0.076)	7.60 (0.27)
Elastic modulus E_{11}, GPa (Mpsi)	39 (5.7)	68 (10.0)
Elastic modulus E_{22}, GPa (Mpsi)	8.6 (1.24)	68 (10.0)
Shear modulus G_{12}, GPa (Mpsi)	3.8 (0.54)	26.2 (3.84)
Major Poisson's ratio, ν_{12}	0.28	0.30
Minor Poisson's ratio, ν_{21}	0.06	0.30
Thermal expansion coefficient α_{11}, 10^{-6}/°C(10^{-6}/°F)	7.0 (3.9)	3.8 (2.1)
Thermal expansion coefficient α^{22}, 10^{-6}/°C(10^{-6}/°F)	21.0 (11.7)	3.8 (2.1)
Piezoelectric charge constant d_{31}, 10^{-12}m/V	0	−125
Electric permittivity ϵ_{33}, 10^{-9}N/V^2	0	11.06
Pyroelectric constant p_3, 10^{-3}C/(m^2°C)	0	−0.25
Reference temperature T_0,°C (°F)	20.0 (68.0)	20.0 (68.0)

Table 2 Convergence studies of beam element

Aspect ratio,	$[0_8/p]$ Open-loop case		$[p/0/90/\pm45]_s$ 100-V case	
L/h	$(u/b) \times 10^3$	$(w/b) \times 10$	$(u/b) \times 10^3$	$(w/b) \times 10$
400	7.93211	3.31520	5.65790	4.52390
200	7.93206	3.31520	5.65680	4.52386
100	7.93193	3.31520	5.65530	4.52382
50	7.93179	3.31520	5.65480	4.52382
25	7.93179	3.31520	5.65475	4.52382

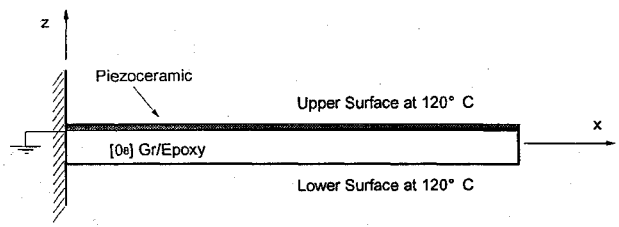

Fig. 1a Composite cantilever $[0_8/p]$ beam under a uniform thermal load.

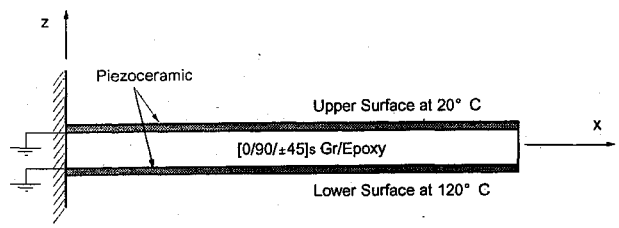

Fig. 1b Composite cantilever $[p/0/90/\pm45]_s$ beam under a thermal gradient.

configuration, which induces thermal distortions under the thermal load. Figures 2 and 3 illustrate the induced axial and transverse displacements produced when the beam is operating in closed circuit conditions. The closed circuit condition is obtained by grounding (0 V) both the lower and upper surfaces of the piezoelectric layer. Grounding both surfaces effectively eliminates the induced piezoelectric strains and produces a virtually conventional composite beam. Thus, the results for this grounded loop condition can also be validated using a conventional finite element structural analysis. This conventional finite element analysis was performed using the MARC[21] analysis code, which operates on an eight processor Cray Y-MP supercomputer. The mesh used for the MARC analysis consists of nine layers of 15 eight-noded quadratic plane stress quadrilateral elements. As shown in Figs. 2 and 3, both methods result in almost identical axial and transverse thermal displacements lending credence to the accuracy of the current formulation.

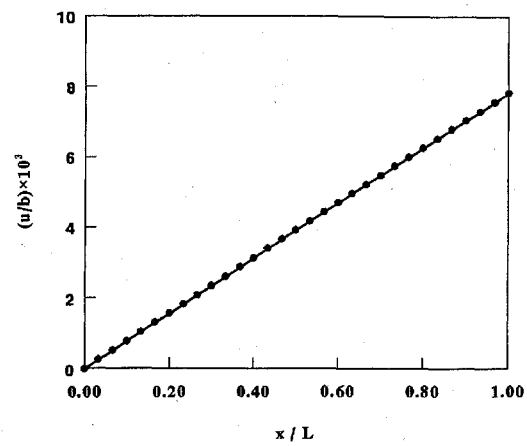

Fig. 2 Axial displacement of a $[0_8/p]$ beam under a uniform thermal load in closed circuit conditions: ——, current FEA and •, MARC FEA.

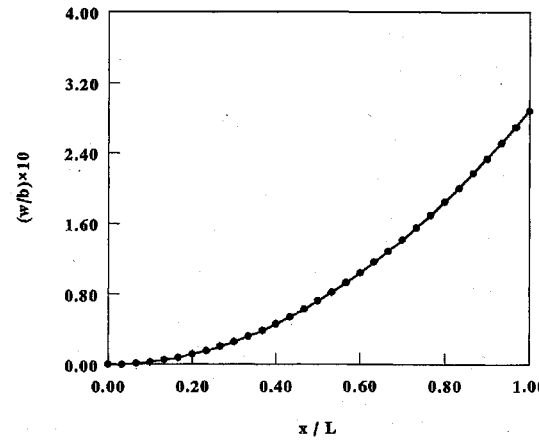

Fig. 3 Transverse displacement of a $[0_8/p]$ beam under a uniform thermal load in closed circuit conditions: ——, current FEA and •, MARC FEA.

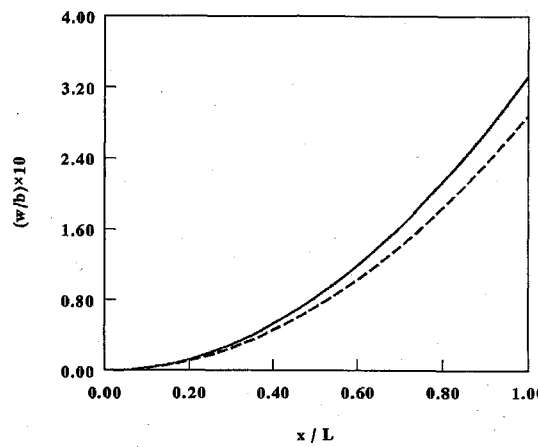

Fig. 4 Effect of electric conditions on the transverse displacement of a $[0_8/p]$ beam under a uniform thermal load: ——, open circuit and – – –, closed circuit.

The resulting transverse thermal deflection of the $[0_8/p]$ beam operating in an open circuit or sensory condition (only the lower surface of the piezoelectric layer is grounded) is shown in Fig. 4. Since only the lower surface is grounded, the effects of the piezoelectrically induced strains are no longer neutralized and lead to the formation of a sensory electric potential on the top surface as a result of the induced thermal stresses. Figure 4 shows a significant difference (~15%) in the transverse displacement between the closed and open circuit conditions. This demonstrates the importance of including the thermoelectrical coupling to model the behavior of thermal

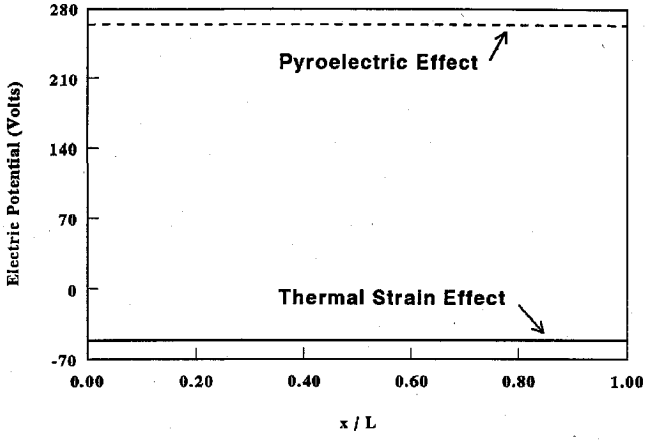

Fig. 5 Predicted sensory electric potential of a $[0_8/p]$ beam under a uniform thermal load.

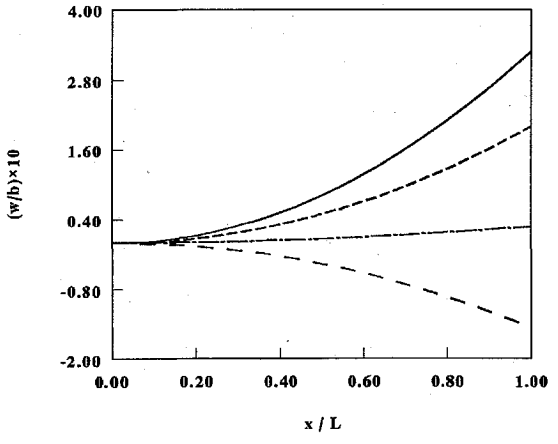

Fig. 6 Active compensation of the transverse displacement of a $[0_8/p]$ beam subjected to a uniform thermal load: ——, open circuit; - - - -, 100 V; – – –, 300 V; and – – –, 500 V.

piezoelectric structures and illustrates the ability of the mechanics to capture this phenomenon.

Sensory Voltage

The open circuit case also demonstrates an important potential application of sensory structures in the monitoring of thermal distortions. In these applications, the displacement fields, which arise under thermal loadings, may be sensed through correlation with the measured voltages at the sensors. This capability is demonstrated in Fig. 5, which shows the measured electric potential (from both the thermal strain and pyroelectric effects) on the top surface corresponding to the transverse displacement shown in Fig. 4. The thermal strain sensory voltage accounts for the effects arising from the thermally induced deformations, while the pyroelectric voltage quantifies the effects that occur because of the variation in temperatures. This application demonstrates the capability to monitor the thermal displacements via the different sensory voltages, which will provide the inferred essential feedback required for thermal distortion management of piezoelectric composite structures.

Thermal Distortion Management

The capability to actively compensate for thermal distortions is demonstrated in Fig. 6 for the $[0_8/p]$ beam. Through application of a voltage differential between the upper and lower surfaces of the piezoelectric layer, the converse piezoelectric effect can be utilized to compensate for the thermal displacements. As shown in the figure, the thermal displacement behavior of the beam can be completely altered from the open-loop state depending on the value of the voltage differential. The thermal distortion can be eliminated by applying a voltage differential of 300 V, whereas a completely

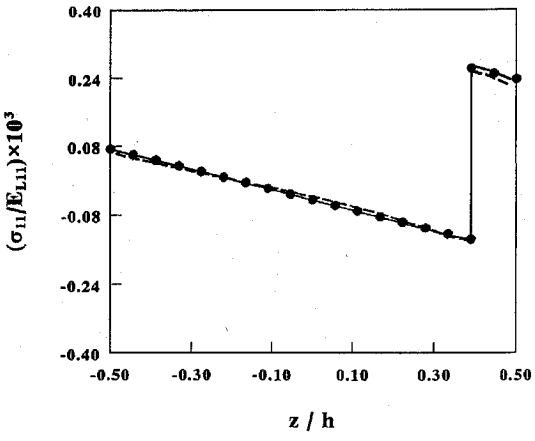

Fig. 7 Axial stress at the middle ($x/L \cong 0.50$) of a $[0_8/p]$ beam under a uniform thermal load in closed circuit conditions: ——, thin beam; – – –, thick beam; and •, CLBT.

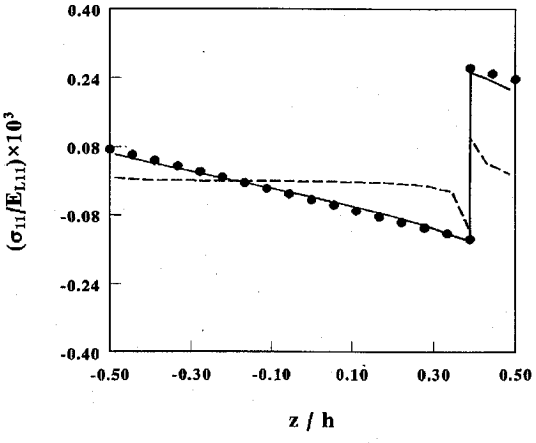

Fig. 8 Axial stress at the end ($x/L \cong 1.0$) of a $[0_8/p]$ beam under a uniform thermal load in closed circuit conditions: ——, thin beam; – – –, thick beam; and •, CLBT.

opposite curvature of the beam can be obtained by applying a voltage differential of 500 V. These results indicate the potential of piezoelectric structures to suppress thermally induced bending.

Thermal Stresses

The stress fields induced in the $[0_8/p]$ beam under closed circuit conditions are shown in Figs. 7–9. The stresses are nondimensionalized using the equivalent laminate moduli E_{L11} and G_{L13}

$$E_{L11} = \frac{1}{h}\int_0^h E_{11}\,dz, \qquad G_{L13} = \frac{1}{h}\int_0^h G_{13}\,dz$$

Stress results are presented from the current finite element formulation and classical beam theory for both thin ($L/h \cong 200$) and thick ($L/h \cong 2$) beams. Figure 7 shows the variation of axial stress (σ_{11}) near the middle of the beam ($x/L \cong 0.5$). There is good agreement between classical beam theory and the current finite element formulation at this location of the beam regardless of the thickness aspect ratio. Notice that an exact solution based on classical laminate beam theory (CLBT) predicts the same stress regardless of the aspect ratio. Figure 8 shows the variation of axial stress (σ_{11}) near the free end of the beam ($x/L \cong 1.0$). At this location, CLBT is accurate only for the low aspect ratio beam. Figure 9 shows the corresponding variation of shear stress (σ_{13}) near the free end of the beam ($x/L \cong 1.0$). CLBT neglects the shear stress, which is only an accurate assumption for the low aspect ratio beam. These results demonstrate the importance of incorporating a refined laminate theory to accurately capture variations of stress through-the-thickness for thick laminates.

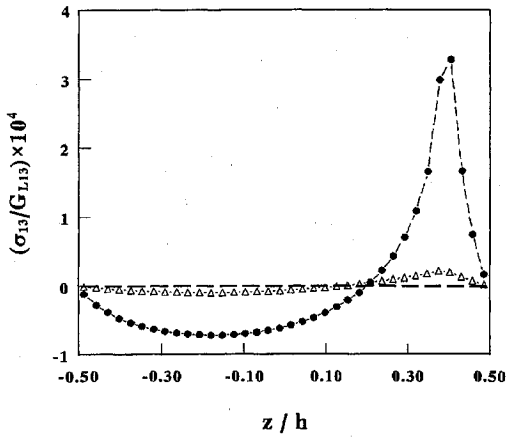

Fig. 9 Shear stress at the end ($x/L \cong 1.0$) of a [$0_8/p$] beam under a uniform thermal load in closed circuit conditions: △, thin beam; •, thick beam; and – – –, CLBT.

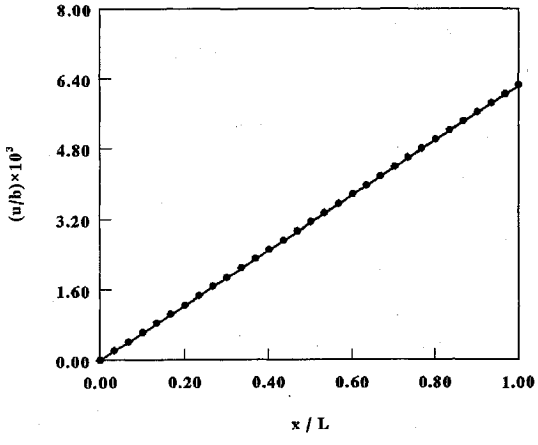

Fig. 10 Axial displacement of a [p/0/90/±45]$_s$ beam under a thermal gradient in closed circuit conditions: ——, current FEA and •, MARC FEA.

[p/0/90/±45]$_s$ *Beam Under Thermal Gradient*

The present example considers multiple piezoelectric layers (to simultaneously take advantage of both the sensory and active behavior of piezoelectric materials), a more general lamination [p/0/90/±45]$_s$, and a through-the-thickness linear thermal gradient (120°C on the bottom surface and 20°C on the top surface) as shown in Fig. 1. Even though the beam has a symmetric laminate configuration including the piezoelectric layers, the applied thermal gradient produces a bending deflection in the beam.

Thermal Displacements

The induced axial and transverse displacements produced in the beam when both piezoelectric layers are operating in closed circuit conditions are shown in Figs. 10 and 11. Also shown are the results from a conventional finite element analysis[21] performed using 10 layers of 15 eight-noded quadratic plane stress quadrilateral elements. Both methods lead to identical predictions, lending credence to the validity to the current formulation.

Combined Sensory and Active Response

In this application, the upper piezoelectric layer is assumed to act as the sensor to monitor the induced electric potential, while the lower piezoelectric layer is used to actively compensate thermal deflections. Figure 12 shows the transverse deflection of the beam under applied voltages of 0, 100, and 200 V on the active (lower) piezoelectric layer. As shown in the figure, increasing the applied voltage reduces the thermally induced deflections from the reference state (0 V). The corresponding sensory electric potentials (from both the thermal strain and pyroelectric effects) measured on the upper piezoelectric layer (sensor) for the different active voltages

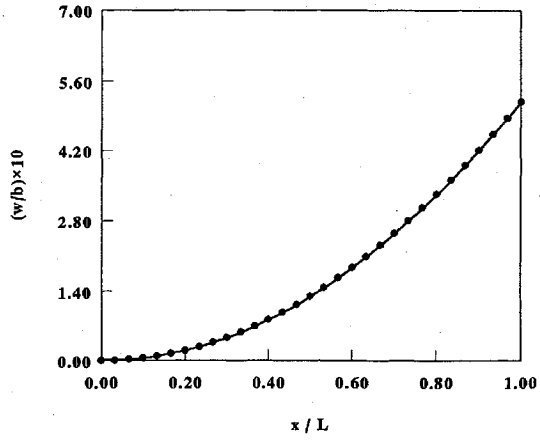

Fig. 11 Transverse displacement of a [p/0/90/±45]$_s$ beam under a thermal gradient in closed circuit conditions: ——, current FEA and •, MARC FEA.

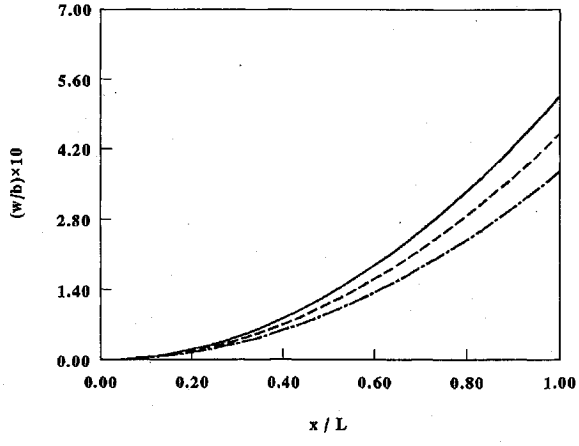

Fig. 12 Active compensation of the transverse displacement of a [p/0/90/±45]$_s$ beam under a thermal gradient: ——, 0 V; – – –, 100 V; and – - – -, 200 V.

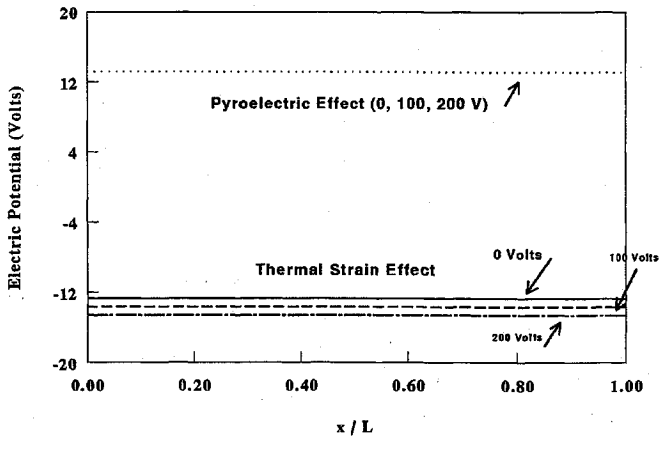

Fig. 13 Predicted sensory electric potential of a [p/0/90/±45]$_s$ beam under a thermal gradient.

are shown in Fig. 13. In actual applications, a control loop would be established between the sensory and active layer, to monitor the sensory voltages and then to generate the appropriate active voltage that will minimize the thermal distortions. This capability is planned to be investigated in the near future.

Thermal Stresses

The axial stress field near the free end ($x/L \cong 1.0$) of the thin [p/0/90/±45]$_s$ beam ($L/h \cong 200$) with an applied voltage of 200 V

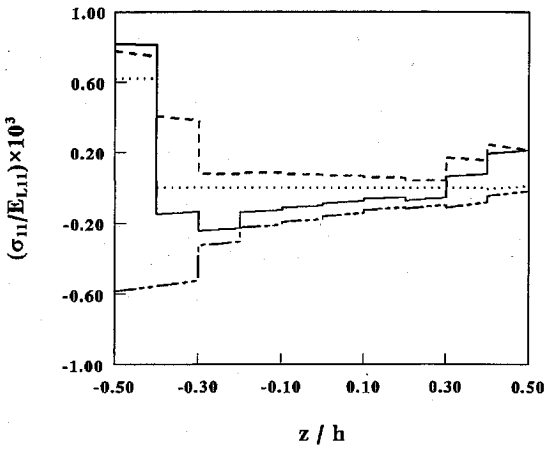

Fig. 14 Axial stress at the middle ($L/h \cong 0.50$) of a $[p/0/90/\pm45]_s$ beam under a thermal gradient: ——, total; – – –, mechanical; — —, thermal; and · · · ·, piezoelectric.

on the bottom piezoelectric layer and the top piezoelectric layer operating in a sensory mode is shown in Fig. 14. The total axial stress is shown together with the three individual components (mechanical, piezoelectric, and thermal), which correspond to the first, second, and third terms on the right-hand side of Eq. (7), respectively. The mechanical component captures the stress resulting from bending, the piezoelectric component arises because of the influence of an electric field on the piezoelectric material, and the thermal component accounts for the stress because of the differences in thermal expansion between plies.

Summary

The development of discrete layer mechanics to model the coupled thermoelectromechanical response of smart thermal composite beams with embedded piezoelectric layers was described. The corresponding finite element formulation was presented, and a linear beam element was developed. The capability of the mechanics to predict the response of piezoelectric composite beams under thermal loadings was demonstrated through numerical studies performed on a $[0_8/p]$ graphite/epoxy beam configured with the piezoceramic layer as either a sensor or an actuator under a uniform thermal load and a $[p/0/90/\pm45]_s$ graphite/epoxy beam with one active and one sensory piezoceramic layer under a thermal gradient. Predicted results for both beams under closed circuit conditions were validated using a conventional finite element analysis.

In addition, the resultant thermal deformations, the corresponding voltage of the piezoceramic sensors, and the internal stress state of the beams were investigated. The capability to actively compensate thermal deflections with piezoceramic actuators was also demonstrated. The numerical studies indicate the significance of thermal effects for piezoelectric composite structures and illustrate the strong coupling between thermal and piezoelectric effects under open circuit conditions. Overall, the case studies have demonstrated the capabilities of the current mechanics to represent the complicated thermomechanical response of thermal piezoelectric composite structures.

References

[1]Bailey, T., and Hubbard, J. E., "Distributed Piezoelectric-Polymer Active Vibration Control of a Cantilever Beam," *Journal of Guidance, Control, and Dynamics*, Vol. 8, No. 5, 1985, pp. 605–611.

[2]Crawley, E. F., and deLuis, J., "Use of Piezoelectric Actuators as Elements of Intelligent Structures," *AIAA Journal*, Vol. 25, No. 10, 1987, pp. 1373–1385.

[3]Tzou, H. S., and Gadre, M., "Theoretical Analysis of a Multi-Layered Thin Shell Coupled with Piezoelectric Shell Actuators for Distributed Vibration Controls," *Journal of Sound and Vibration*, Vol. 132, No. 3, 1989, pp. 433–450.

[4]Lee, C.-K., Chiang, W.-W., and O'Sullivan, T. C., "Piezoelectric Modal Sensor/Actuator Pairs for Critical Active Damping Vibration Control," *Journal of the Acoustical Society of America*, Vol. 90, No. 1, 1991, pp. 374–384.

[5]Wang, B.-T., and Rogers, C. A., "Laminate Plate Theory for Spatially Distributed Induced Strain Actuators," *Journal of Composite Materials*, Vol. 25, No. 4, 1991, pp. 433–452.

[6]Allik, H., and Hughes, T. J. R., "Finite Element Method for Piezoelectric Vibration," *International Journal for Numerical Methods in Engineering*, Vol. 2, No. 2, 1970, pp. 151–157.

[7]Naillon, M., Coursant, R. H., and Besnier, F., "Analysis of Piezoelectric Structures by a Finite Element Method," *Acta Electronica*, Vol. 25, No. 4, 1983, pp. 341–362.

[8]Tzou, H. S., and Tseng, C. I., "Distributed Piezoelectric Sensor/Actuator Design for Dynamic Measurement/Control of Distributed Parametric Systems: A Piezoelectric Finite Element Approach," *Journal of Sound and Vibration*, Vol. 138, No. 1, 1990, pp. 17–34.

[9]Lammering, R., "The Application of a Finite Shell Element for Composites Containing Piezoelectric Polymers in Vibration Control," *Computers and Structures*, Vol. 41, No. 5, 1991, pp. 1101–1109.

[10]Ha, S. K., Keilers, C., and Chang, F.-K., "Finite Element Analysis of Composite Structures Containing Distributed Piezoceramic Sensors and Actuators," *AIAA Journal*, Vol. 30, No. 3, 1992, pp. 772–780.

[11]Reddy, J. N., "A Generalization of Two-Dimensional Theories of Laminated Composite Plates," *Communications in Applied Numerical Methods*, Vol. 3, 1987, pp. 173–180.

[12]Robbins, D. H., and Reddy, J. N., "Analysis of Piezoelectrically Actuated Beams Using a Layer-Wise Displacement Theory," *Computers and Structures*, Vol. 41, No. 2, 1991, pp. 265–279.

[13]Heyliger, P., Ramirez, G., and Saravanos, D. A., "Coupled Discrete Layer Finite Elements for Laminated Piezoelectric Plates," *Communications in Numerical Methods in Engineering*, Vol. 10, 1994, pp. 971–981.

[14]Saravanos, D. A., and Heyliger, P. R., "Coupled Electromechanical Response of Composite Beams with Embedded Piezoelectric Sensors and Actuators," *Journal of Intelligent Material Systems and Structures*, Vol. 6, No. 3, 1995, pp. 350–363; also NASA CR 195313, June 1994.

[15]Mindlin, R. D., "Equations of High Frequency Vibrations of Thermopiezoelectric Crystal Plates," *International Journal of Solids Structures*, Vol. 10, No. 6, 1974, pp. 625–632.

[16]Tauchert, T. R., "Piezothermoelastic Behavior of a Laminated Plate," *Journal of Thermal Stresses*, Vol. 15, No. 1, 1992, pp. 25–37.

[17]Rao, S. S., and Sunar, M., "Analysis of Distributed Thermopiezoelectric Sensors and Actuators in Advanced Intelligent Structures," *AIAA Journal*, Vol. 31, No. 7, 1993, pp. 1280–1286.

[18]Tzou, H. S., and Howard, R. V., "A Piezothermoelastic Thin Shell Theory Applied to Active Structures," *Journal of Vibration and Acoustics*, Vol. 116, No. 3, 1994, pp. 295–302.

[19]Tzou, H. S., and Ye, R., "Piezothermoelasticity and Precision Control of Piezoelectric Systems: Theory and Finite Element Analysis," *Journal of Vibration and Acoustics*, Vol. 116, No. 4, 1994, pp. 489–495.

[20]Nye, J. F., *Physical Properties of Crystals*, Clarendon, Oxford, England, UK, 1964.

[21]Anon., MARC Reference Library Volumes A–D, Version K 5.2, MARC Analysis Research Corp., Palo Alto, CA, 1992.